Permeability Estimations of SMC Material Particles

Joonas Vesa[1] and Paavo Rasilo[1]
[1]Unit of Electrical Engineering, Tampere University, Tampere, 33720 Finland

In this study we estimate the locally defined permeability of the magnetizing particles in a soft magnetic composite (SMC) material whose effective permeability, observed by macrosopic measurements, is known. This procedure is repeated for a wide range of geometries whose electrical insulation layer thicknesses between the magnetizing particles are altered. It is shown that even if the effective permeability of the material is known by some measurement, the permeabilities of the individual particles cannot be immediately determined but remain heavily dependent on the thicknesses of the insulation films. This dependency is quantified. It is shown that when using periodic geometries to imitate SMC materials, one also has to use higher local permeabilities for the magnetizing particles or thinner insulations between the particles compared to the situation where randomized structures are used, in order to obtain the effective permeability determined by measurements.

***Index Terms*—B-H Curve, Geometry generation, Magnetic contact, Material identification, Soft magnetic composite, Voronoi tessellation.**

I. Introduction

SOFT magnetic composite (SMC) materials consist of ferromagnetic particles, possibly mixed with an electrical insulation material, compressed and annealed. SMC materials are advantageous in terms of isotropy and low eddy current losses [1], [2].

Modeling of SMC materials is not straightforward, since they are multiscale by nature. The individual ferromagnetic particles in the materials are small, often some tens of micrometers in diameter, and eddy current losses are affected by the geometry of this scale. On the other hand, the particle scale geometry of the material cannot be entirely included into a computational model, since computational resources are limited. In Fig. 1a, we see a microscope image of an SMC material.

Various different computational studies of SMC materials exist. Prof. Igarashi *et al.* have quite some experience of such studies [3], [4], [5], [6], [7]. Waki *et al.* carried out a comparative study of predicting effective permeabilities of materials with arbitrary inclusions on 2-D cells [3]. The study included a nonlinear consideration. Ito *et al.* considered SMC materials with periodic symmetry consisting of homogeneous magnetic bricks [4]. Sato *et al.* proposed methods for computing hysteresis and eddy current losses in SMC materials [5]. Ito *et al.* considered the meaning of magnetic contacts in terms of understanding the numerical values of the effective permeabilities of SMC materials [6]. Maruo *et al.* performed an analysis of SMC materials based on the discrete element method [7]. The paper is considered particularly interesting, since it included a mechanical simulation of random packing of round grains.

It is also worth mentioning the work done in VTT [8] and the papers of Belkadi *et al.* related to automatic geometry generation [9], [10]. Their papers along with the works of Prof. Igarashi *et al.* have been the primary inspiration for our studies.

We have focused on SMC geometry generation and estimation methods in 3-D. In our previous publication, our approach of constructing geometries was presented [11]. In Fig. 1b, we see one such geometry imitation. Various different

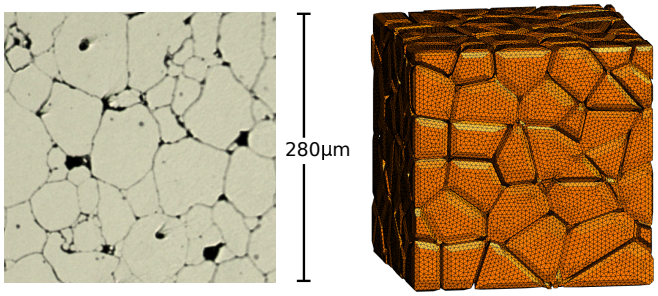

(a) Microscope image (b) Generated geometry

Fig. 1. (a) A microscope image of a Fe-Ni-Mo alloy SMC [11] [12]. (b) A generated imitation of an SMC material geometry.

features of the geometries, such as the volume fraction of the magnetizing particles and insulation thicknesses between individual particles, can be controlled. It was established that a measurement of a nonlinear effective B-H curve of an SMC material could be repeated computationally very accurately regardless of whether neighbouring magnetizing particles are in mechanical contact or sharing thin insulation layers in between. The key difference in these two cases was that the estimated locally defined B-H curves had significant differences in the unsaturated region. We could loosely say that if low external magnetic field was applied, the permeability of the particles turned out to be sensitive to the contact vs. thin insulation -property of the geometry. It was speculated that there exists a wide range of geometries and corresponding locally defined magnetizing characteristics, such that they provide computational results consistent with the measurements.

This paper is going to give evidence that such an assertion holds. Since the differences were the most drastic in

Manuscript received March 31, 2020; revised ????? ?, 2020. Corresponding author: J. Vesa (https://tutcris.tut.fi/portal/en/persons/joonas-vesa(c7791107-71f3-413e-a85e-f8b4b7424509).html).

the unsaturated region, in this paper we concentrate on the low-field characteristics of the material. Moreover, we are going to quantify the dependency between the locally defined permeability of the magnetizing particles and the thickness of the insulation layers between the particles in the material while keeping the effective permeability of the material consistent with measurements. For the nonlinear analysis, the reader is directed to the original results [11].

II. Measurements

As a sample, we use a Magnetics Inc. C055106A2 MPP core, which is a Fe-Ni-Mo alloy based SMC. The cross-sectional image in Fig. 1a is taken from this material. In the datasheet the relative permeability was reported to be $\mu_{\mathrm{r,eff}} = 200$ [12]. To measure the effective $B-H$ loop, a two-coil measurement setup was utilized. The current of the primary coil was measured over one period of 50 Hz continuous excitation. The voltage of the open secondary coil was measured over one period as well. The magnetic field strength was solved from the primary current and the magnetic flux density was calculated from the integral of the secondary voltage.

The measurements are depicted in Fig. 2 and an additional line, representing a linear approximation with permeability $\mu_{\mathrm{r,eff}} = 200$, is plotted. Hysteresis is low. Hence, we say that the material experiences relative permeability of $\mu_{\mathrm{r,eff}} = 200$ at least if the magnetic flux density is less than 0.3 T in magnitude.

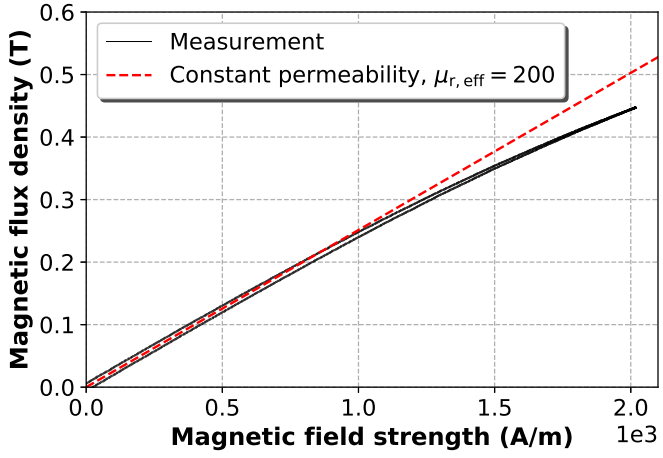

Fig. 2. Effective $B-H$ curve of the material in Fig. 1a.

III. Problem definition

In order to express the problem in an intuitive manner and to provide a test bench for a finite element (FE) model, we state the problem first as a very much simplified problem in 1-D. Treating such a problem is easy. Then, we extend the same problem into 3-D and use the existing methods of geometry generation in order to study it in the context of SMC materials.

A. Simplified example

As depicted in Fig. 3, we consider a 1-D bar of length l containing magnetizing linear matter, with relative permeability μ_{r}, and non-magnetic material of length xl, with x as a dimensionless parameter describing the insulation thickness. The bar is magnetized along its length. Since the normal

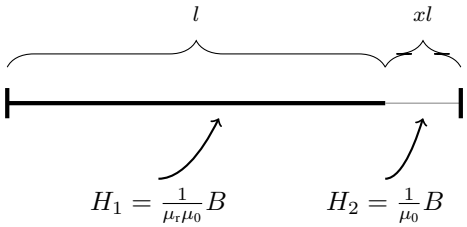

Fig. 3. Simplified 1-D problem.

component of the magnetic flux density B is continuous, it is constant all over the bar. Effective magnetic field strength H is defined as the total magnetomotive force over the bar, divided by $(1+x)l$. Hence, inserting the constitutive equations in Fig. 3 into $H = \frac{1}{(1+x)l}\left(lH_1 + xlH_2\right)$ and performing obvious manipulations yields

$$B = \underbrace{\frac{1+x}{\frac{1}{\mu_{\mathrm{r}}}+x}}_{=:\mu_{\mathrm{r,eff}}}\mu_0 H, \tag{1}$$

where $\mu_{\mathrm{r,eff}}$ is an effective relative permeability. Solving for μ_{r}, gives

$$\mu_{\mathrm{r}}(x) = \frac{1}{\frac{1+x}{\mu_{\mathrm{r,eff}}} - x}. \tag{2}$$

The quantity $\mu_{\mathrm{r,eff}}$ is a measurement value. In our case, as in Fig. 2, we set $\mu_{\mathrm{r,eff}} = 200$. What is left in (2), is a relation between the locally defined permeability μ_{r} and the 'insulation thickness factor' x. Consistency with the measurement requires choosing x and μ_{r} such that the relation holds. We notice that it must hold that $x < \frac{1}{\mu_{\mathrm{r,eff}}-1}$, or the effective permeability $\mu_{\mathrm{r,eff}}$ cannot be met whatever positive value μ_{r} gets. In Fig. 4, a portion of the graph of the relation (2) is depicted. The FE model points in the Fig. will be discussed later.

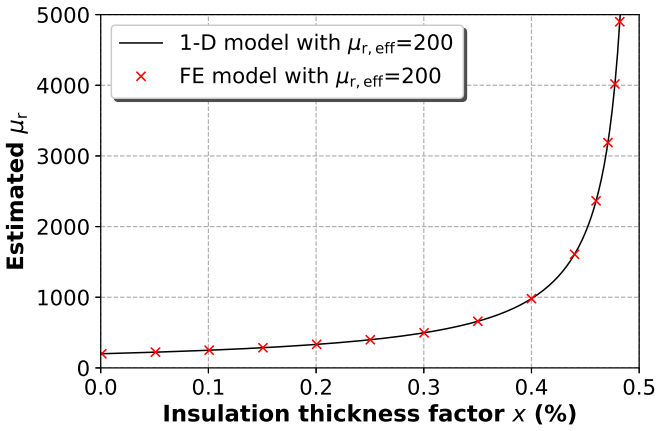

Fig. 4. Relation (2).

The central problem we investigate in this paper is to find a wide range of 3-D imitations of SMC geometries with various insulation thicknesses that together with corresponding locally defined permeabilities μ_{r} yield effective permeabilities for the material strictly consistent with the measurement. It is expected that the insulation thickness vs. permeability relations will have the same overall shape as in Fig. 4.

Another problem we study in order to assess the reliability of the results, is the sensitivity of the locally defined 'estimated' permeability μ_{r}. Let us first consider again the simplified problem. Let us define a relative error of μ_{r}. We set

$$e(x, \Delta x) := \frac{\mu_{\mathrm{r}}(x + \Delta x) - \mu_{\mathrm{r}}(x)}{\mu_{\mathrm{r}}(x)}. \tag{3}$$

The quantity Δx is a dimensionless number representing a small 'measurement error' of x meaning that the permeability estimation is simulated in a situation where the insulation thickness has been addressed in an inaccurate manner. This kind of misaddressing of a distributed gap in an SMC material is quite an obvious issue since the material geometries are very random and stochastic by nature.

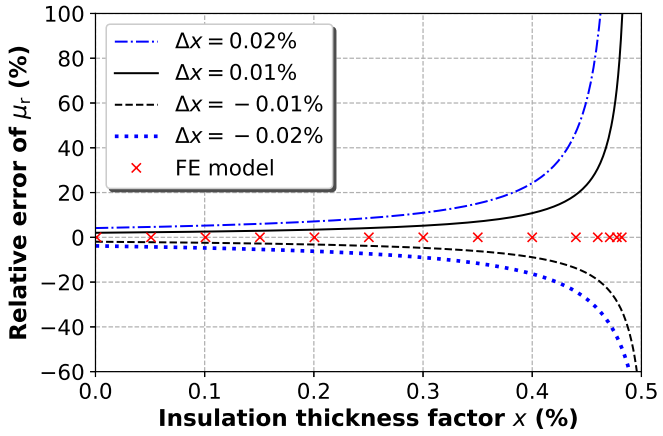

Fig. 5. Error (3) of μ_{r}, depicted in Fig. 4, computed using various errors of the insulation thickness factor x. Note that x and Δx are dimensionless numbers and hence, both x and Δx can be expressed as percents, as fractions of one hundred. The quantity Δx still represents absolute error of x even though expressed in percents.

In Fig. 5, we have depicted the error (3) with several different absolute errors in the insulation thickness factor x. We notice that the relative error e increases rapidly as the factor x increases. The FE model points in the figure are discussed later.

The secondary problem in this paper is to study how the randomization of the SMC geometries yields uncertainty to the locally defined 'estimated' μ_{r}. It is expected that in a similar fashion as in Fig. 5, the uncertainty of μ_{r} raises as the insulation thicknesses in the geometries increase. We also study how increasing the particle number in the geometry cell decreases the uncertainty.

B. 3-D problem

Using the methods described in our previous work, geometries may be generated by defining suitable parameters. If the reader feels uncomfortable reading the following considerations, we advice reading the definition of the geometry generation [11]. In a nutshell, the geometries are generated inside the cubical cell $[0, 1]^3$. Then the following parameters are given. First, a number N is given, determining the number of particles in the cell. In Fig. 1b, the number is 216. Second, a floating point number d is given. A randomized process places N points inside the cube $[0, 1]^3$ under the restriction that each point has to be at least the distance d away from each other. Then, a Voronoi tessellation for the cell $[0, 1]^3$ is computed from these points. Finally, two vectors, w_{F} and w_{C} are given, w_{F} defining how the cell faces are refined and w_{C} determining how the refined faces are contracted inside each cell to form gaps between the particles. Finally, the geometry, or the computational mesh defined on it, is scaled appropriately.

Let us generate two sets of geometries. As a starting point we use the parameters that were used previously [11]. The

TABLE I
GEOMETRY TEMPLATE I

N	$3^3 = 27$
d	0.45/3
w_{F}	[0,0.4]
w_{C}	[0.1,0]

TABLE II
GEOMETRY TEMPLATE II

N	$6^3 = 216$
d	0.45/6
w_{F}	[0,0.4]
w_{C}	[0.1,0]

parameters for the first set of geometries are given in Table I. The geometries have 27 particles and a volume fraction $V_{\mathrm{F}} = 0.9$. In addition, the particles have a contact surface fraction of $S_{\mathrm{F}} = 0.36$, which means that 36 % of their surface area is in contact with neighbouring particles. Two hundred geometries were generated using randomized voronoi tessellations. One such geometry is depicted on the left-hand side of Fig. 6.

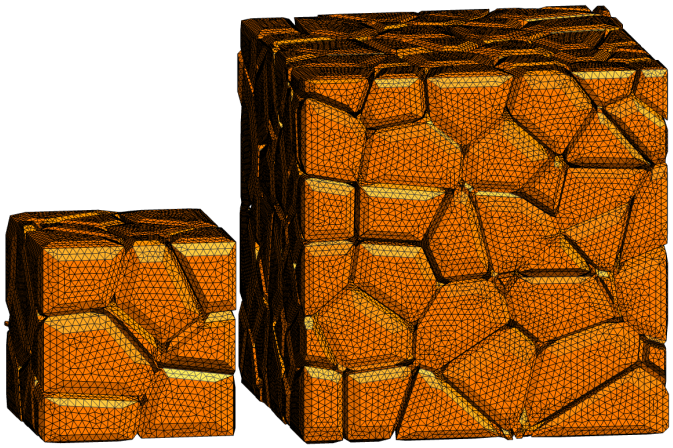

Fig. 6. Geomerty on the left is generated using the parameters in Table I and it contains 3^3 particles. Its mesh contains about 30 000 nodes in 230 000 elements. The geometry on the right is generated using the parameters in Table II and it contains 6^3 particles. Its mesh contains about 240 000 nodes in 1 900 000 elements.

Another set of two hundred randomized geometries was generated based on the parameters in Table II. The key difference between the geometries based on Tables I and II is the number of particles inside the cell. The first set contains 3^3 particles inside each geometry and the second set contains 6^3

particles inside each geometry. One sample of the geometries with 6^3 particles is depicted on the right-hand side of Fig. 6.

In this study we estimate the locally defined permeabilities of the particles of the generated geometries such that computations of effective permeabilities yield the measured value $\mu_{\text{r,eff}} = 200$. The aim is to carry out similar computations to the depicted ones in Figs 4 and 5 but in a more realistic setting. Electrical insulation layers are introduced in the model using degenerate prisms with adjustable thicknesses between the particles. Details of the computational model will be discussed next.

IV. Computational methods

Let us consider a geometry, for instance the right one in Fig. 6. It is much like the simplified schematic image in Fig. 7. The

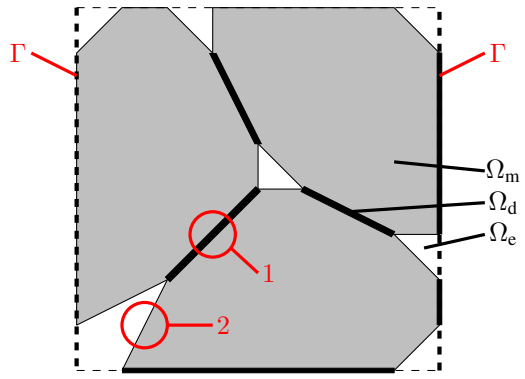

Fig. 7. A schematic of the geometries.

geometry would be meshed with tetrahedra. In the schematic Fig. 7, the grey areas represent the magnetizing particles and the white areas are insulation. The bold black lines, denoted by the number 1 in the figure, represent thin insulations between the particles. The thin insulations on the boundary of the whole domain are placed such that for each two opposite faces of the boundary only one has thin insulations and not the other.

These thin insulations are not meshed in 3-D using an automated mesh generator but degenerate prisms are used. Abenius *et al.* described the use of degenerate prisms in the setting of edge basis [13]. We use an approach similar to these ideas but with a practical simplification. Instead of operating in the prisms using 2-D basis functions, we embed the information about small thicknesses of the prisms into the change of coordinates mappings of the degenerate prisms.

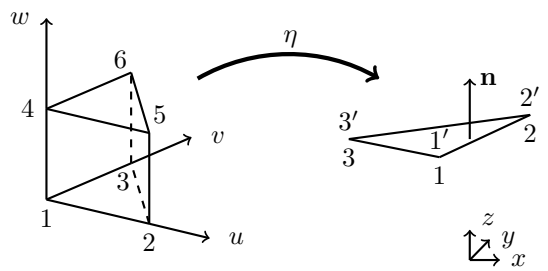

Fig. 8. Change of coordinates from a reference prism to a degenerate prism.

In Fig. 8 we see a change of coordinates mapping η from a reference prism to a degenerate prism. The mapping is given by

$$\eta : (u, v, w) \longmapsto \sum_{i=1}^{3} N_i(u, v)\mathbf{x}^i + tw\mathbf{n}, \tag{4}$$

where N_1, N_2 and N_3 are the nodal shape functions of the triangle $1-2-3$ in the reference plane uv, $\mathbf{x}^i$ are the coordinates of the ith node of the degenerate prism, t is the desired thickness of the degenerate prism and $\mathbf{n}$ is the unit normal vector of the degenerate prism. Adjusting t, one can adjust the insulation thicknesses of the material. Effectively the prisms are just right-angled prisms and the concrete computations of the FE method may be performed on the reference prism.

We denote the whole domain inside the dashed square in Fig. 7 by Ω_w, the magnetizing regions by Ω_m, white empty regions by Ω_e and thin insulation regions, modeled by degenerate prisms, by Ω_d. We set the FE problem on the domain $\Omega := \Omega_m \cup \Omega_d$ ignoring Ω_e. In addition, a condition $\mathbf{B} \cdot \mathbf{n} = 0$ is set on the layers between Ω_e and Ω_m, denoted by the number 2 in Fig. 7. This assumption relies on two facts. First, the permeability ratio between Ω_m and Ω_e is at least 200. It means that the magnetic field tends to traverse through the magnetizing particles avoiding non-magnetizing regions. Second, the thicknesses of the empty regions Ω_e are substantially higher than the thickness of the thin insulations Ω_d. Hence, the magnetic field tends to pass from one particle to another via the thin insulation regions and not the thick empty regions.

In the domain Ω it holds that

$$\nabla \cdot \mu \left(\mathbf{H}_{\text{ext}} + \nabla\varphi\right) = 0, \tag{5}$$

where φ is a scalar potential to be solved, $\mu = \mu_0$ in Ω_d, $\mu = \mu_r\mu_0$ in Ω_m, where μ_r is an input value to the model and $\mathbf{H}_{\text{ext}}$ is a constant excitation field in the direction of one of the coordinate basis vectors. Let us choose a unit excitation $\mathbf{H}_{\text{ext}} = H_{\text{ext}}\mathbf{e}_1$ with $H_{\text{ext}} = 1$ A/m and set $\varphi = 0$ on Γ, with Γ as in Fig. 7. The model accepts μ_r as an input, solves (5) in Ω by Galerkin FE method with nodal scalar basis for φ. Now the magnetic field is given by $\mathbf{H} = \mathbf{H}_{\text{ext}} + \nabla\varphi$ and $\mathbf{B} = \mu\left(\mathbf{H}_{\text{ext}} + \nabla\varphi\right)$. As in the works of Niyonzima *et al.*, the effective fields $\langle\mathbf{B}\rangle$ and $\langle\mathbf{H}\rangle$ are obtained by averaging $\mathbf{B}$ and $\mathbf{H}$ over the domain Ω_w, respectively [14]. Since $\langle\nabla\varphi\rangle = 0$ due to the chosen Dirichlet condition, $\varphi = 0$ on Γ, the average of $\mathbf{H} = \mathbf{H}_{\text{ext}} + \nabla\varphi$ is just a unit $\langle\mathbf{H}\rangle = \langle H_{\text{ext}}\mathbf{e}_1\rangle = H_{\text{ext}}\mathbf{e}_1$. On the other hand, the average of $\mathbf{B}$ is

$$\frac{1}{|\Omega_w|}\int_{\Omega} \mathbf{B}\mathrm{dV}, \tag{6}$$

where the integration is reduced to Ω, since $\mathbf{B}$ is assumed to be low in Ω_e due to the high permeability ratio between the magnetizing and empty regions. The effective permeability $\mu_{\text{r,eff}}$ is given by

$$\langle\mathbf{B}\rangle \cdot \mathbf{e}_1 = \mu_{\text{r,eff}}\mu_0\left(\langle\mathbf{H}\rangle \cdot \mathbf{e}_1\right). \tag{7}$$

The forward model F takes the locally defined μ_r as an input and returns the effective $\mu_{\text{r,eff}}$. We solve for μ_r from

$F(\mu_r) = 200$ using the modified Powell method implemented in the Scipy root package [15].

As a simplified trial case for validating the computational model, we choose the simple geometry in Fig. 9. The ge-

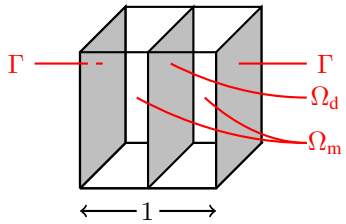

Fig. 9. Simplified geometry for validating the computational model.

ometry was meshed into 8958 tetrahedra with 1562 nodes, and degenerate prisms were defined on Ω_d. Various insulation thicknesses were chosen, and relative permeabilities μ_r were estimated for the magnetizing regions Ω_m assuming the effective relative permeability to be 200. The results were plotted into Fig. 4 as 'FE model' with the insulation thickness factor x in the plots set directly as the insulation thickness t in the FE model. In the error plot in Fig. 5, the finite element computations were compared with the analytical solution (2). There is no discrepancy between the analytical and the FE solution.

V. Computational results

Let us begin by analyzing the two hundred SMC geometries with 27 particles, one of which is depicted on the left-hand side of Fig. 6. Permeability estimations were carried out for the two hundred geometries with various different insulation thicknesses t described in Section IV. Each estimation presented in the following considerations converged and effective relative permeability of 200 was met by an absolute tolerance of 10^{-6}.

The estimated relative permeabilities μ_r are depicted in Fig. 10a with red dots and a label 'Randomized, $N = 3^3$'. The meaning of the number 3^3 is that there are $3^3 = 27$ particles in each geometry. The plot is made against a scaled insulation thickness, denoted by $3t$. The idea here is that if the particles in the geometry were arranged to a periodic $3 \times 3 \times 3$-array, there would be three insulation layers for the magnetic field to pass and the quantity $3t$ describes the total amount of insulation that the field must pass in order to travel from one face of the geometry to the opposite. The insulation thickness is expressed as a percentage of the total width of the geometry.

The reader is warned about some red dots soaring out of the scale of the plot in the region of insulation thickness $3t \geq 0.16\%$. This can be seen from the light red patch containing all the red dots, labeled as 'Patch of randomized, $N = 3^3$'. The patch diverges and crosses the relative permeability 5000 before the 0.16% thickness. However, due to high deviation in the estimated permeabilities in this region, the results with insulation thicknesses this high are already unusable. In Fig. 10a is also depicted the mean of the estimated local relative permeabilities for each insulation thickness labeled as 'Mean of randomized, $N = 3^3$'.

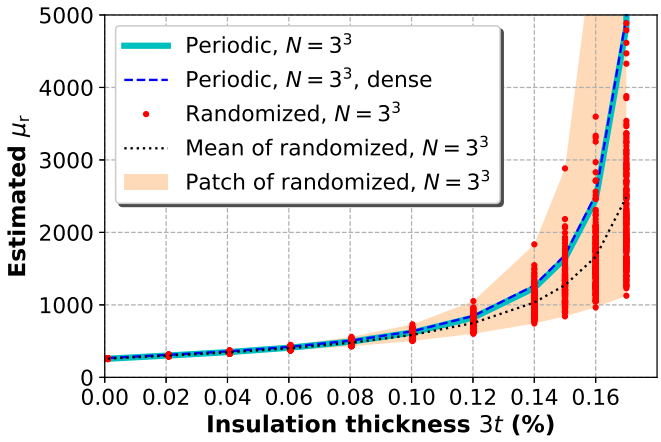

(a) Estimated permeabilities

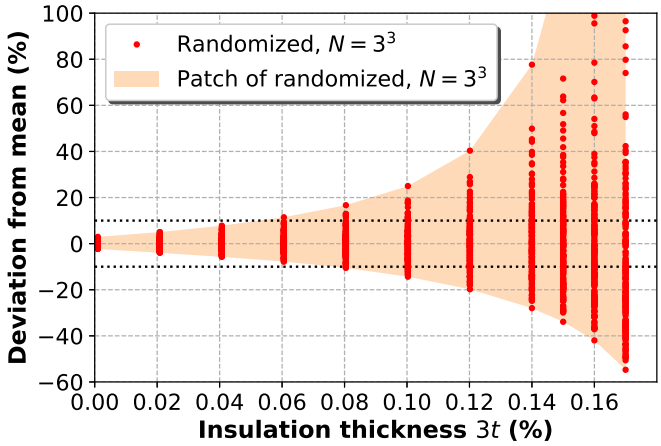

(b) Deviation of estimated permeabilities

Fig. 10. Estimation results using the geometries with 27 particles.

Fig. 10b demonstrates how each estimated permeability μ_r deviates from the mean, depicted in Fig. 10a. For a fixed insulation thickness, denote the mean by $\mu_{r,mean}$ and one of the two hundred estimated permeabilities as $\mu_{r,i}$ with i denoting the geometry. The deviation from mean is defined by

$$\frac{\mu_{r,i} - \mu_{r,mean}}{\mu_{r,mean}}. \tag{8}$$

The deviations are depicted as red dots in Fig. 10b, labeled as 'Randomized, $N = 3^3$', and the patch, 'Patch of randomized, $N = 3^3$' contains all the results. In Fig. 10b, there is also a 10% band, depicted by the dashed horizontal lines. If maximum 10% discrepancy is accepted for the estimated permeabilities from the mean of the estimated permeabilities, the computations with insulation thickness only up to approximately $3t = 0.06\%$ would be acceptable. This is not a particularly good result and later in this paper, we seek for an enhancement by considering geometries with substantially more particles.

Comparing the results depicted in Figs 10a and 10b to the results in Figs 4 and 5, respectively, we see that the results have the same overall trends. When the insulation thicknesses and estimated relative permeabilities increase, the deviation in the estimated relative permeabilities rises.

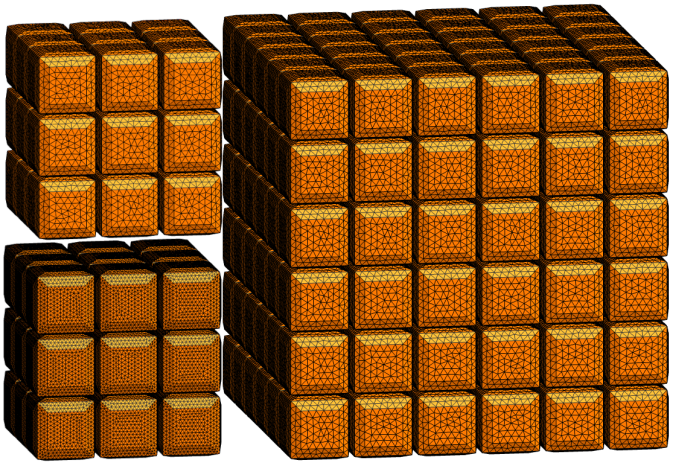

Fig. 11. The geomerty on the upper left is generated using the parameters in Table I and it contains 3^3 particles. Its mesh contains about 23 000 nodes in 175 000 elements. The geomerty on the lower left is generated using the parameters in Table I and it contains 3^3 particles. Its mesh contains about 105 000 nodes in 737 000 elements. The geometry on the right is generated using the parameters in Table II and it contains 6^3 particles. Its mesh contains about 174 000 nodes in 1 370 000 elements.

In Fig. 10a, there are two additional lines, labeled as 'Periodic, $N = 3^3$' and 'Periodic, $N = 3^3$, dense'. These results are obtained by repeating the computations for the upper left and lower left geometry in Fig. 11, respectively. The geometries are the same but the mesh density is different. The geometries are obtained by the same parameters defined in Table I, but the underlying tessellation consists of a periodic array of cubes. What we see in Fig. 10a is that the results obtained using the two different meshes of periodic geometry are independent of mesh. According to the considerations in Section III-A, the deviation of the results is expected to increase when the relative permeability of the magnetizing particles and the insulation thicknesses are large. It seems that the mesh has very little effect in this deviation. This suggests that the results are reliable in terms of discretization errors.

Let us now repeat the computations using geometries with $6^3 = 216$ particles. Figs 12a and 12b contain analogous results to the Figs 10a and 10b. This time the randomized geometries are much like the one sample on the right-hand side of Fig. 6 and the periodic geometry is depicted on the right-hand side of Fig. 11. We see that the overall trend of the results in Fig. 12 are consistent with the results in Fig. 10, but there is far less deviation. In this case, less than 10% deviation is achieved with insulation thicknesses up to 0.13 % of the original width of the geometry. If even thicker insulations were to be considered, we would expect increasing the particle number in the representative cell further to decrease the deviation even more.

For comparison, in Fig. 12a there is a curve 'Periodic, $N = 3^3$', which was depicted earlier in Fig. 10a. This curve is very close to the curve 'Periodic, $N = 6^3$', obtained using a periodic geometry with 216 particles. We conclude that in the periodic case, the results are independent of the number of particles contained in the inclusion.

In Fig. 12a it is obvious that the periodic geometries yield estimated permeabilities far higher than the randomized

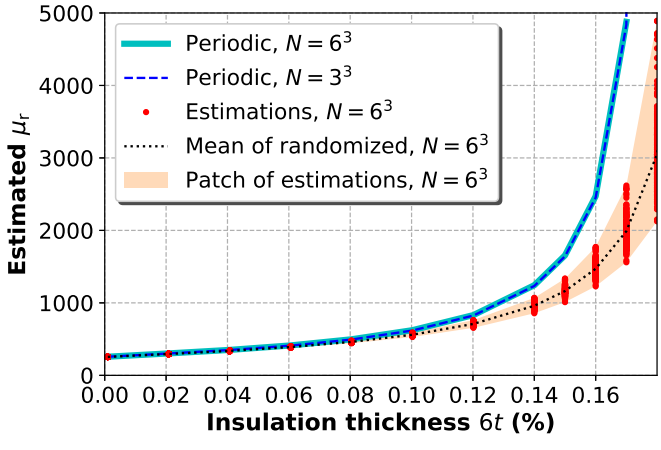

(a) Estimated permeabilities

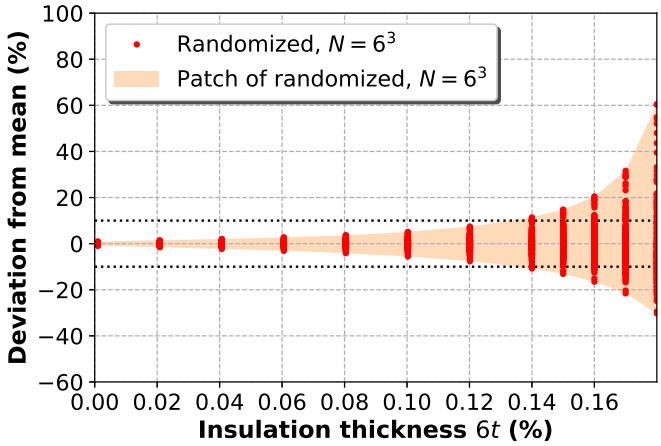

(b) Deviation of estimated permeabilities

Fig. 12. Estimation results using the geometries with 216 particles.

geometries. This trend is visible also in the results in Fig. 10a but not as obviously. The explanation for such a result is simple. Consider the randomized geometry on the left-hand side of Fig. 6. It is possible to pass from the left face of the whole geometry to the right face of the geometry by passing just two particles and two insulations. Considering the cubical geometry on the left-hand side of Fig. 11, it is only possible to travel from the left face of the whole geometry to the right face of the geometry by passing three particles and three insulations. Hence, in the periodic case, there are more insulation layers to be passed. If the effective relative permeability is fixed to the measured value 200, either the locally defined permeability must be higher or the insulation layers must be thinner in the periodic case.

VI. Concluding Remarks

In this paper we studied the dependency between the insulation layer thicknesses of an SMC material and the locally defined permeability of the magnetizing particles. The effective permeability of the material was kept strictly consistent with a measured value. The study was conducted using an automatic SMC geometry generation tool with control over the

volume fraction, particle number and insulation thicknesses of the geometry.

It was demonstrated that a measurement of the effective permeability of an SMC material does not determine the permeability of the material particles and the thicknesses of the electrical insulations between the particles uniquely. Instead, it was shown that these quantities are dependent of each other and this dependency was quantified. With randomized structures, the uncertainties in the estimated permeabilities increased as the insulation thicknesses increased. This uncertainty was reduced by increasing the number of particles in the inclusions.

It was shown that using periodic geometries, either the relative permeabilities of the particles must be higher or the electrical insulations thinner compared to the corresponding quantities in randomized geometries in order to achieve the same effective permeability. This is a consequence of the periodic geometries suffering from a larger amount of insulations to be passed by the magnetic field.

ACKNOWLEDGMENT

The foundation of Emil Aaltonen and the Academy of Finland are acknowledged for financial support. J. Vesa thanks his sister Saara Göös for reading the paper and commenting on the style.

REFERENCES

[1] H. Shokrollahi and K. Janghorban, "Soft magnetic composite materials (SMCs)", *Journal of Materials Processing Technology*, vol. 189, Feb. 2007.

[2] K. Sunday and M. Taheri, "Soft magnetic composites: recent advancements in the technology", *Metal Powder Report*, vol. 72, no. 6, Nov./Dec. 2017.

[3] H. Waki, H. Igarashi, and T. Honma, "Estimation of Effective Permeability of Magnetic Composite Materials", *IEEE Transactions on Magnetics*, vol. 41, no. 5, May. 2005.

[4] Y. Ito and H. Igarashi, "Computation of Macroscopic Electromagnetic Properties of Soft Magnetic Composite", *IEEE Transactions on Magnetics*, vol. 49, no. 5, May. 2013.

[5] T. Sato, S. Aya, H. Igarashi, M. Suzuki, Y. Iwasaki, and K. Kawano, "Loss Computation of Soft Magnetic Composite Inductors Based on Interpolated Scalar Magnetic Property", *IEEE Transactions on Magnetics*, vol. 51, no. 3, Mar. 2015.

[6] Y. Ito, H. Igarashi, M. Suzuki, Y. Iwasaki and K. Kawano, "Effect of Magnetic Contact on Macroscopic Permeability of Soft Magnetic Composite", *IEEE Transactions on Magnetics*, vol. 52, no. 3, Mar. 2016.

[7] A. Maruo and H. Igarashi, "Analysis of Magnetic Properties of Soft Magnetic Composite Using Discrete Element Method", *IEEE Transactions on Magnetics*, vol. 55, no. 6, Jun. 2019.

[8] Multiscale modelling and design for engineering application, *VTT Technology 77*, Kopijyvä Oy, Kuopio 2013.

[9] M. Belkadi, B. Ramdane, D. Trichet and J. Fouladgar, "Non Linear Homogenization for Calculation of Electromagnetic Properties of Soft Magnetic Composite Materials", *IEEE Transactions on Magnetics*, vol. 45, no. 10, Oct. 2009.

[10] M. Belkadi, D. Trichet, B. Ramdane and J. Fouladgar, "Modeling of Soft Magnetic Composite Material Using a Non Linear Homogenization Method", *Proc. CEFC*, Chigago, IL, USA, May 2010.

[11] J. Vesa and P. Rasilo, "Producing 3-D Imitations of Soft Magnetic Composite Material Geometries", *IEEE Transactions on Magnetics*, vol. 55, no. 10, Oct. 2019.

[12] Magnetics Inc. C055106A2 datasheet, Revision Nov. 2016, https://www.mag-inc.com/Media/Magnetics/Datasheets/C055106A2.pdf.

[13] E. Abenius and F. Edelvik, "Thin Sheet Modeling Using Shell Elements in the Finite-Element Time-Domain Method", *IEEE Transactions on Antennas and Propagation*, vol. 54, no. 1, Jan. 2006.

[14] I. Niyonzima, R. V. Sabariego, P. Dular, C. Geuzaine, "Finite Element Computational Homogenization of Nonlinear Multiscale Materials in Magnetostatics", *IEEE Transactions on Magnetics*, vol. 48, no. 2m Feb. 2012.

[15] Scipy scipy.optimize.root documentation, Cited in Mar. 2020, https://docs.scipy.org/doc/scipy/reference/optimize.root-hybr.html#optimize-root-hybr.